Standardization of Reporting Criteria for Lung Pathology in SARS-CoV-2–infected Hamsters: What Matters?

To the Editor:

Respiratory failure because of severe lung pathology is the prime indication for emergency care and decisive for disease outcome in patients with coronavirus disease (COVID-19). Though clinical and computed tomography data are widely accessible, limited autopsy data are available where comorbidities may confound the spectrum of lesions (1, 2). However, a detailed understanding of viral spread, target cells and organs, time-dependent tissue damage, inflammatory responses, and regeneration and repair is essential for optimal clinical management and the development of preventive and therapeutic measures. In particular, disease mechanisms beyond classical pneumonia play a serious role in COVID-19, including vascular lesions (1, 3).

For elucidation and the testing of drugs and vaccines, a suitable animal model is needed urgently. As mice are not naturally susceptible to severe acute respiratory syndrome coronavirus 2 (SARS-CoV-2), several transgenic models and viral vectors have been developed that express the human ACE2 receptor (4). However, the outcome of infections varied depending on model-specific artificial expression levels and cellular distributions of the transgenic receptor, which still limits their interpretability. Besides less practical alternatives including primates (5–7), the Syrian hamster is emerging as a popular naturally susceptible small animal model. Importantly, first histopathology reports revealed several similarities to pulmonary changes observed in patients with COVID-19 (8–10). However, microscopic descriptions mentioned only select facets of the complex changes and used divergent nomenclatures, which makes comparisons and interpretations of the different studies difficult. Moreover, a systematic comparison to what is known of human COVID-19 pneumonia is lacking. Clearly, the reporting criteria for lung pathology patterns need to be harmonized with an agreement on what is relevant for humans before hamsters can be beneficial in preclinical studies. After all, among other functional, cellular and molecular, and more measurable parameters, histological evidence of tissue injury is viewed as the most relevant defining feature of acute lung injury by the American Thoracic Society (11).

Standardized evaluation criteria for proven or potentially important diagnostic parameters are useful as guidelines for the harmonization, comparability, reproducibility, and robustness of diverse studies aiming at understanding disease mechanisms and testing vaccines or novel therapeutic strategies, and they are particularly useful for meta-analyses. Such a catalog of significant, evidence-based histopathology patterns from systematic comparisons, and their relevance for different applications, was previously established and repeatedly applied to a wide spectrum of mouse models of pneumonia (12). Here, we propose such a catalog for the reporting of histopathology in SARS-CoV-2–infected hamsters (Table 1) that is based on our previous observations (13) and systematic comparisons with other reports on SARS-CoV-2–infected hamsters (8–10), macaques (6, 7), and lesions considered relevant in humans (1–3). Table 1 highlights both the disparity between previous reports on hamsters as well as similarities to and differences from patients with COVID-19. We illustrated our catalog with microphotographs (Figure 1) of the most prominent lesions in hamsters and side-by-side comparisons with similar lesions in humans. Localization of viral RNA by *in situ* hybridization allows for a concomitant appraisal of the presence of the virus in hamsters (Figures 1W–1Z).

The list of relevant lesions (Table 1) and the hamster microphotographs (Figure 1) resulted from a comprehensive study with 24 intranasally infected Syrian hamsters of different ages. Time points of clinical, virological, and pathological examinations ranged from 2 to 14 days postinfection (dpi). Methods are given in the data supplement, and more detailed results were published elsewhere (13).

Our study revealed that the observability of most parameters depends on several determinants, primarily the time point after infection. For example, a necrosuppurative bronchitis at 2 dpi turned into a bronchointerstitial pneumonia at 3 dpi. By 5 dpi, a patchy, largely interstitial pneumonia was present with onset of repair and regeneration, followed by almost complete recovery at 14 dpi. Other determinants include the age of the animals (13) and infectious dose used (10). Supposedly, the occurrence, severity, and time course of the different patterns will also be affected by therapeutic interventions and vaccines. Endothelialitis, which is considered important in patients (3) but not previously reported in hamsters, was consistently observed in our study at 5 dpi, albeit without detectable viral RNA in endothelial cells (Figure 1Z). The documentation of endothelialitis clearly increases the value of the hamster model. Also, our finding that young hamsters launch an earlier, stronger, and obviously more effective immune response than older hamsters do (13) makes this model attractive for investigating this issue of high relevance in humans. Likewise, a strong and early influx of granulocytes resembling bacterial infection was observed in our hamsters as described in patients (1, 13). On the other hand, microvascular thrombosis and angiogenesis, both considered relevant in COVID-19 (3), were not yet observed in Syrian hamsters. Nevertheless, lesions with known relevance for patients should be included in such a list with guideline significance to point out differences that could be model specific. Certainly, as our understanding of COVID-19 pathology will increase with time, the catalog of parameters proposed here should be considered preliminary and subject to amendments whenever justified.

Supported by COVID-19 funds by Freie Universität Berlin and the Berlin University Alliance (N.O.) and Einstein Foundation fund EZ3R-2020–597FU, BMBF Grant ORGANO-STRAT and German Research Foundation Grant SFB-TR84/Z01b (A.D.G.).

Author Contributions: A.D.G. and K.D. designed the study, examined lung tissues, interpreted data, and wrote the manuscript. N.O., L.D.B., D.V., and J.T. designed and conducted the animal experiments, processed samples, and acquired and interpreted data. S.G., J.I., and D.H. contributed and interpreted human pathology data.

This letter has a data supplement, which is accessible from this issue's table of contents at www.atsjournals.org.

Originally Published in Press as DOI: 10.1165/rcmb.2020-0280LE on September 8, 2020

Table 1. Proposed Reporting Criteria for SARS-CoV-2–induced Pneumonia as Seen in Hamsters, Macaques, and Patients with COVID-19

Histopathological Pattern/Parameter	Observed in Our Hamster Study (13)	Reported in SARS-CoV-2–infected Hamsters	Reported in SARS-CoV-2–infected Macaques	Reported in Patients with COVID-19
Overall severity				
% of lung area affected	5–95	(9, 10)	—	—
Distribution of lesions				
Bronchial and peribronchial	+	(10)	—	(1)
Patchy throughout the lungs	+	(8–10)	(7)	(2, 3)
Cell and tissue damage				
Necrosis of BEC	+	(9)	(6)	—
Cellular debris in bronchi	+	(9)	—	—
Diffuse alveolar damage	+	(9)	(6)	(1–3)
Necrosis of AEC	+	(9)	(6)	(3)
Hyaline membranes	—	(9)	(6)	(1, 2)
Cellular debris in alveoli	+	(9)	(6, 7)	—
Intraalveolar fibrin deposition	—	—	(6)	(3)
Alveolar emphysema	+	(8)	—	—
Circulatory changes and vascular lesions				
Alveolar hemorrhage	+	(8, 9)	—	+
Alveolar edema	+	(8, 9)	(6, 7)	(2, 3)
Perivascular/interstitial edema	+	—	—	(1, 3)
Microvascular thrombosis	—	—	—	(1, 3)
Vascular endothelialitis	+	—	(6)	(3)
Necrosis and desquamation of vascular endothelial cells	+	—	—	(3)
Reactive inflammatory patterns				
Necrosuppurative bronchitis	+	—	—	—
Bronchointerstitial pneumonia	+	(9)	(6)	—
Interstitial pneumonia	+	(8)	(7)	(2)
Intraalveolar neutrophils and macrophages	+	(8)	(6, 7)	(1)
Marked involvement of:				
Lymphocytes	+	—	(7)	(1, 2)
Polymorphonuclear granulocytes (neutrophils, heterophils)	+	—	(6)	(1)
Monocytes, macrophages	+	—	(7)	—
Perivascular lymphocytic cuffing	+	—	(6)	(3)
Activation of mesothelial cells	+	—	—	—
Regeneration and repair				
Hyperplasia of BEC	+	(9, 10)	(6)	—
Hyperplasia of AEC-II	+	(9, 10)	(6)	(1–3)
Multinucleated or otherwise atypical epithelial cells	+	(9)	(6)	(1, 2)
Pleural fibroblastic proliferation/fibrosis	+	—	—	+
Angiogenesis	—	—	—	(3)
Localization of SARS-CoV-2 in				
BEC	+	(8–10)	(6)	—
AEC-I	+	(8–10)	(6, 7)	—
AEC-II	+	(8–10)	(6, 7)	—
Alveolar macrophages	+	—	(7)	—
Vascular endothelial cells	—	—	—	(3)

Definition of abbreviations: AEC = alveolar epithelial cells; BEC = bronchial epithelial cells; COVID-19 = coronavirus disease; SARS-CoV-2 = severe acute respiratory syndrome coronavirus 2.

Patterns highly characteristic of SARS-CoV-2–induced pneumonia in hamsters and/or relevant in human patients with COVID-19 are highlighted in boldface. References in parentheses refer to previous reports.

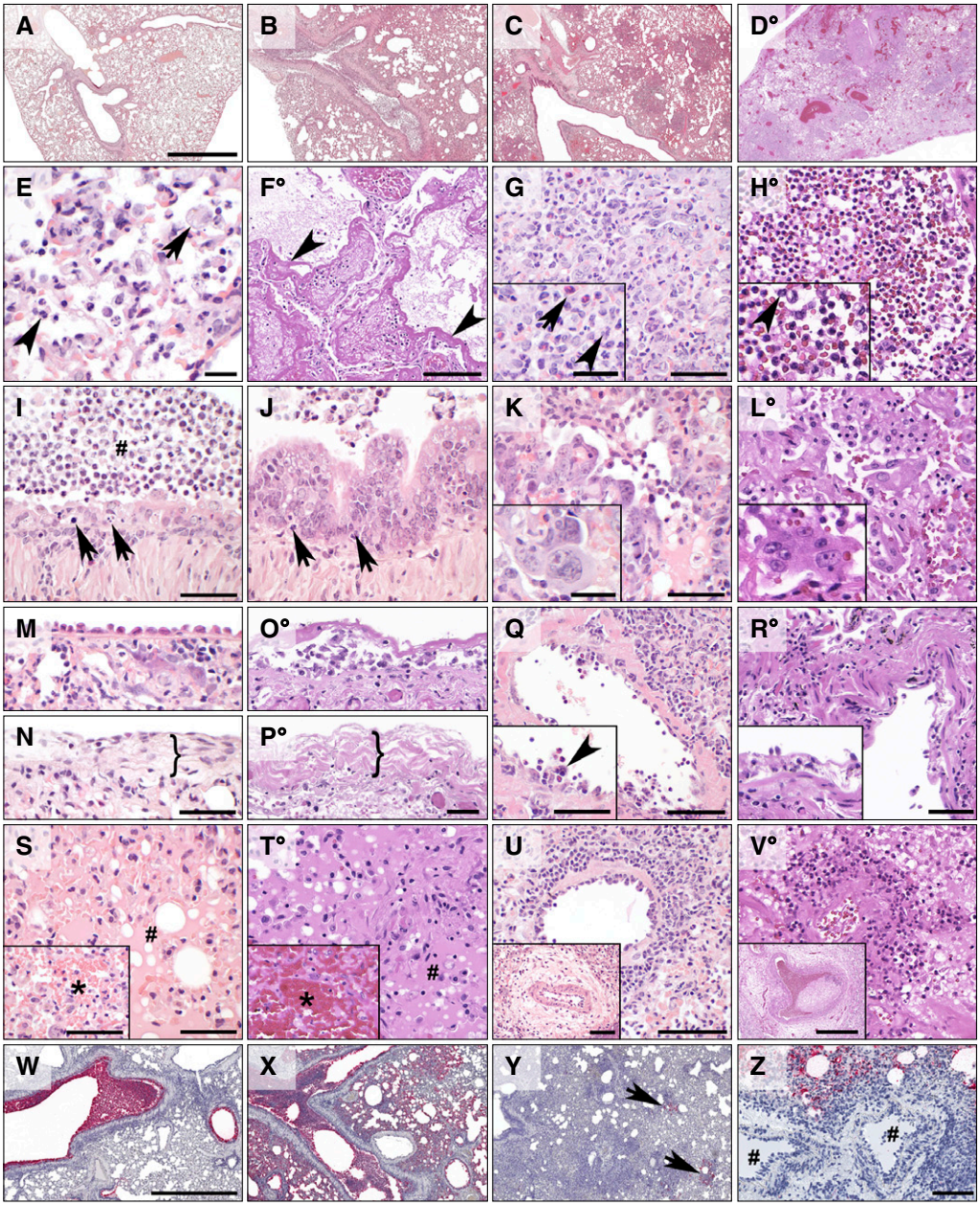

Figure 1. Characteristic histopathological patterns in severe acute respiratory syndrome coronavirus 2 (SARS-CoV-2)–induced pneumonia in Syrian hamsters and humans (° = human specimens). (*A–D)* In hamsters, a strongly time-dependent distribution of lesions started solely bronchially at 2 days postinfection (dpi) (*A*), turned into bronchointerstitial at 3 dpi (*B*), and into a patchy, purely interstitial pneumonia from 5 dpi onward (*C*), which is also characteristic in humans (*D*). (*E* and *F*) A consistent feature in both was acute diffuse alveolar damage, including necrosis of alveolar epithelial cells, hyaline membranes (*F*, arrowhead), intraalveolar macrophages (*E*, arrow), neutrophils (*E*, arrowhead), and cellular debris. (*G* and *H*) Starting at 5 dpi in hamsters, interstitial pneumonia (*G*) with notably high involvement of neutrophils (inset, arrowhead) and heterophils (inset, arrow) was present, similar to strong granulocytic infiltrations in humans (*H*, inset, arrowhead). (*I* and *J*) Marked bronchitis (*I*) with necrosis of bronchial epithelial cells (arrows) and intraluminal neutrophils with cellular debris (hash symbol) dominated at early time points in hamsters, followed by strong regeneration characterized by massive hyperplasia of bronchial epithelium (*J*, arrows indicate mitotic figures). (*K* and *L*) In both hamsters and humans, hyperplasia of alveolar type II epithelial cells with bizarre multinucleated cellular atypia (insets) was prominent. (*M–O*) Pleural changes included cuboidal activation of mesothelial cells (*M*), multifocal pleural fibrosis (*N* and *P*, bracket symbols), and pleuritis (*O*). (*Q–V*) Vascular pathology included endothelialitis (*Q* and *R*) with necrosis and desquamation of endothelial cells (*Q*, inset, arrowhead), alveolar edema (*S* and *T*, hash symbols), and hemorrhage (insets, asterisks) as well as perivascular lymphocytic cuffing (*U* and *V*) and edema (insets). (*A–V*), hematoxylin and eosin stains of formalin-fixed, paraffin-embedded tissues. (*W–Y*) Viral RNA as detected in hamsters by *in situ* hybridization preceded inflammatory reactions in a time-dependent manner, starting with high abundance only in bronchi at 2 dpi (*W*), spreading to the lung periphery at 3 dpi (*X*), and finally turning into a purely interstitial patchy pattern with less signals at 5 dpi (*Y*). (*Z*) Endothelialitis had no detectable viral RNA (hash symbols). Red, signals for viral RNA; blue, hemalaun counterstain. Scale bars: *A–D*, 2 mm; *E*, 20 μm; *F*, *Q*, *U*, and *V*, 200 μm; *G–O*, *S*, and *T*, 50 μm; *P*, *R*, and *Z*, 100 μm; *W–Y*, 1 mm. Scale bars in insets: *G*, *H*, *K*, and *L*, 50 μm; *R*, *Q*, *S*, *T*, and *U*, 100 μm; *V*, 500 μm.

Applications in which standardized evaluation criteria will be beneficial particularly include assessments of the prophylactic or therapeutic efficacy of candidate vaccines or drugs that are on their way (14). In addition, the list can be helpful in determining differences in the virulence of virus isolates, effects of infectious dosage, comorbidities, age, or differences to other models including transgenic mice (4). In all scenarios, distinct study goals may justify different choices among the patterns proposed here. For example, perivascular lymphocytic cuffs may be relevant for the assessment of specific immune responses, as expected from vaccine trials, whereas aspects of regeneration and repair may be important age-related parameters. For any kind of comparative study, a bouquet of histologic quantification tools is already available that convert differences in each morphological parameter into statistically testable data, including scoring schemes (12), Cavalieri's principle (15), and computed digital image analyses (16).

We are only at the beginning of our understanding of COVID-19. The application of a structured, evidence-based catalog of relevant diagnostic criteria will certainly increase the value of information that can be obtained from animal models. ■

Author disclosures are available with the text of this letter at www.atsjournals.org.

Achim D. Gruber, D.V.M., Ph.D.*
Nikolaus Osterrieder, D.V.M.
Luca D. Bertzbach, D.V.M., Ph.D.
Daria Vladimirova, D.V.M.
Freie Universität Berlin
Berlin, Germany

Selina Greuel, M.D.
Jana Ihlow, M.D.
David Horst, M.D.
Charité–Universitätsmedizin Berlin
Berlin, Germany

Jakob Trimpert, D.V.M.‡
Kristina Dietert, D.V.M., Ph.D.‡
Freie Universität Berlin
Berlin, Germany

ORCID IDs: 0000-0002-4502-0393 (A.D.G.); 0000-0002-5313-2176 (N.O.); 0000-0002-0698-5395 (L.D.B.); 0000-0002-1562-4268 (D.V.); 0000-0001-5346-4499 (S.G.); 0000-0001-5484-1321 (J.I.); 0000-0003-4755-5743 (D.H.); 0000-0003-1616-0810 (J.T.); 0000-0002-5667-6750 (K.D.).

*Corresponding author (e-mail: achim.gruber@fu-berlin.de).
‡These authors contributed equally to this work.

References

1. Wichmann D, Sperhake JP, Lütgehetmann M, Steurer S, Edler C, Heinemann A, *et al*. Autopsy findings and venous thromboembolism in patients with COVID-19. *Ann Intern Med* [online ahead of print] 6 May 2020; DOI: 10.7326/M20-2003.
2. Hanley B, Lucas SB, Youd E, Swift B, Osborn M. Autopsy in suspected COVID-19 cases. *J Clin Pathol* 2020;73:239–242.
3. Ackermann M, Verleden SE, Kuehnel M, Haverich A, Welte T, Laenger F, *et al*. Pulmonary vascular endothelialitis, thrombosis, and angiogenesis in COVID-19. *New Engl J Med* 2020;383:120–128.
4. Le Bras A. Modeling SARS-CoV-2 infection in mice. *Lab Anim (NY)* 2020; 49:198.
5. Cleary SJ, Pitchford SC, Amison RT, Carrington R, Robaina Cabrera CL, Magnen M, *et al*. Animal models of mechanisms of SARS-CoV-2 infection and COVID-19 pathology. *Br J Pharmacol* [online ahead of print] 27 May 2020; DOI: 10.1111/bph.15143.
6. Rockx B, Kuiken T, Herfst S, Bestebroer T, Lamers MM, Oude Munnink BB, *et al*. Comparative pathogenesis of COVID-19, MERS, and SARS in a nonhuman primate model. *Science* 2020;368:1012–1015.
7. Yu P, Qi F, Xu Y, Li F, Liu P, Liu J, *et al*. Age-related rhesus macaque models of COVID-19. *Animal Model Exp Med* 2020;3:93–97.
8. Sia SF, Yan LM, Chin AWH, Fung K, Choy KT, Wong AYL, *et al*. Pathogenesis and transmission of Sars-CoV-2 in golden hamsters. *Nature* 2020;583:834–838.
9. Chan JF, Zhang AJ, Yuan S, Poon VK, Chan CC, Lee AC, *et al*. Simulation of the clinical and pathological manifestations of coronavirus disease 2019 (COVID-19) in golden syrian hamster model: implications for disease pathogenesis and transmissibility. *Clin Infect Dis* [online ahead of print] 26 Mar 2020; DOI: 10.1093/cid/ciaa325.
10. Imai M, Iwatsuki-Horimoto K, Hatta M, Loeber S, Halfmann PJ, Nakajima N, *et al*. Syrian hamsters as a small animal model for SARS-CoV-2 infection and countermeasure development. *Proc Natl Acad Sci USA* 2020;117:16587–16595.
11. Matute-Bello G, Downey G, Moore BB, Groshong SD, Matthay MA, Slutsky AS, *et al*.; Acute Lung Injury in Animals Study Group. An official American Thoracic Society workshop report: features and measurements of experimental acute lung injury in animals. *Am J Respir Cell Mol Biol* 2011;44:725–738.
12. Dietert K, Gutbier B, Wienhold SM, Reppe K, Jiang X, Yao L, *et al*. Spectrum of pathogen- and model-specific histopathologies in mouse models of acute pneumonia. *PLoS One* 2017;12:e0188251.
13. Osterrieder N, Bertzbach LD, Dietert K, Abdelgawad A, Vladimirova D, Kunec D, *et al*. Age-dependent progression of sars-cov-2 infection in syrian hamsters. *Viruses* 2020;12:779.
14. Kreye J, Reincke SM, Kornau HC, Sanchez-Sendin E, Corman VM, Liu H, *et al*. A SARS-CoV-2 neutralizing antibody protects from lung pathology in a COVID-19 hamster model. *Cell* [online ahead of print] 23 Sep 2020; DOI: 10.1016/j.cell.2020.09.049.
15. Dietert K, Reppe K, Mundhenk L, Witzenrath M, Gruber AD. mCLCA3 modulates IL-17 and CXCL-1 induction and leukocyte recruitment in murine Staphylococcus aureus pneumonia. *PLoS One* 2014;9:e102606.
16. Dietert K, Nouailles G, Gutbier B, Reppe K, Berger S, Jiang X, *et al*. Digital image analyses on whole-lung slides in mouse models of acute pneumonia. *Am J Respir Cell Mol Biol* 2018;58:440–448.

Effects of Asthma and Human Rhinovirus A16 on the Expression of SARS-CoV-2 Entry Factors in Human Airway Epithelium

To the Editor:

The factors that facilitate and impact transmission of the severe acute respiratory syndrome coronavirus 2 (SARS-CoV-2) are not well understood, particularly in children and young adults. It has been established that the S (Spike) protein of SARS-CoV-2 binds to ACE2 (angiotensin-converting enzyme 2) as the entry receptor and employs the serine protease TMPRSS2 for proteolytic separation of

Supported by U.S. National Institutes of Health Grants U19AI125378 (S.F.Z.), K24AI150991 (J.S.D.), R01HL089215, and K24AI130263 (T.S.H.).

Originally Published in Press as DOI: 10.1165/rcmb.2020-0394LE on September 18, 2020